Inorganic Chemistry

Article

pubs.acs.org/IC

Mechanism of Water Oxidation to Molecular Oxygen with Osmocene as Photocatalyst: A Theoretical Study

Yue Chen, Juan Han, and Wei-Hai Fang*

College of Chemistry, Beijing Normal University, Beijing 100875, People's Republic of China

Supporting Information

ABSTRACT: In the present work, photoinduced O_2 evolution from the $[Cp_2Os{-}OH]^+$ complex in aqueous solution has been studied by the DFT, CASSCF, and CASPT2 methods. The CASPT2//CASSCF calculations predict that the S_3 state is initially populated and the subsequent deprotonation of $[Cp_2Os{-}OH]^+$ proceeds very easily along the T_1 pathway as a result of the efficient $S_3 \rightarrow T_1$ intersystem crossing. It is found that the O−O bond is formed via the acid−base mechanism, which is different from the direct oxo−oxo coupling mechanism suggested in the experimental study. Formation of the O−O bond is the rate-determining step and has an activation energy and activation free energy of 81.3 and 90.4 kcal/mol, respectively. This is consistent with the low quantum yield observed for generating molecular oxygen upon irradiation at 350 nm (∼ 82 kcal/mol). The O_2 release from an intermediate complex has to overcome a small barrier on the triplet pathway first and then pass through the triplet−singlet intersection, generating the O_2 molecules in either the lowest singlet or triplet state. The formed $^3O_2$ molecule can be converted into the $^1O_2$ molecule by the heavy atom effect in the Os complexes, which is probably the reason only the $^1O_2$ molecule was detected experimentally.

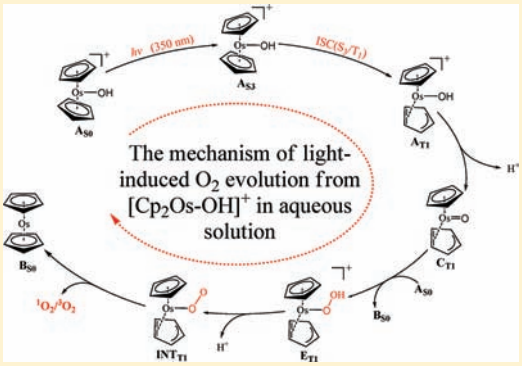

INTRODUCTION

Catalytic water oxidation to molecular oxygen is of fundamental importance to natural and artificial photosynthesis. The direct sunlight-driven splitting of water into O_2 and H_2 is anticipated as one of the most promising strategies for providing environmentally friendly and renewable energy sources.[1−6] In the past several decades, intense research efforts have been pursued to develop both heterogeneous and molecular catalysts that enable water oxidation.[7−15] Enormous progress has been made in the field of artificial photosynthesis that uses semiconductors and electrolysis.[3,4,16,17] In recent years, molecular catalysts for water oxidation have received a considerable amount of attention. Molecular systems can be studied mechanistically and can be tailored both structurally and electronically, which gives them an advantage over heterogeneous systems and allows for a more systematic approach in the design of new generations of water oxidation catalysts.[5,18,19]

Since the first functional Ru-based water oxidation catalyst, "blue dimer", was reported by Meyer and co-workers,[20] the Ru, Mn, Ir, Ce, and Os complexes have received a great deal of attention with respect to the design of new transition-metal complexes as the homogeneous catalytic systems.[8,21−29] A few molecular catalysts were reported that use UV light as the driving force to oxidize the water into O_2 without sacrificial oxidants. Since there is no electron transfer between catalyst and sacrificial oxidants in these systems, their reaction mechanisms are expected to be different from those of water oxidation by oxidants. Milstein and co-workers designed a very different reaction scheme in which a consecutive thermal H_2 and light-induced O_2 evolution from water was promoted by a Ru(II) hydride hydroxo complex.[30−33] The subsequent articles[34,35] highlighted the great potential of this reaction scheme for water splitting, although the overall reaction is actually slow with rather low yields for the H_2 and O_2 generation.[30] The H_2 release was predicted to have a barrier of ∼35 kcal/mol by DFT (density functional theory) calculations,[32] which might be the reason for the slow H_2 generation. H_2O_2 was suggested as an important intermediate for the O_2 formation,[30] which is not supported by the DFT calculations.[31,33] A new mechanism was proposed for formation of the triplet O_2 molecule, where the O−O bond is formed along the T_1 pathway as a result of efficient $S_1 \rightarrow T_1$ intersystem crossing.[33]

Vogler and co-workers utilized osmocene (Cp_2Os^{II}, Cp = $C_5H_5^-$) as a photocatalyst to split water into H_2 and O_2 via two purely photochemical reactions.[36] The first reaction yields the H_2 molecule by irradiation of osmocene in acidic aqueous solution, and the H_2 release was suggested by dimeric $[Cp_2Os^{IV}H\cdots HOs^{IV}Cp_2]$ units. The second reaction generates molecular oxygen by photolysis of the $[Cp_2Os^{IV}OH]^+(PF_6)^-$ complex in aqueous solution. A nearly quantitative conversion of $[Cp_2Os^{IV}OH]^+$ to O_2 and Cp_2Os^{II} was observed, and the peroxo complex $[Cp_2Os^{III}(O_2)Os^{III}Cp_2]$ was suggested as a transient intermediate for the O_2 release. These two separate

Received: September 26, 2011
Published: April 9, 2012

   dx.doi.org/10.1021/ic202097c | Inorg. Chem. 2012, 51, 4938−4946

Scheme 1

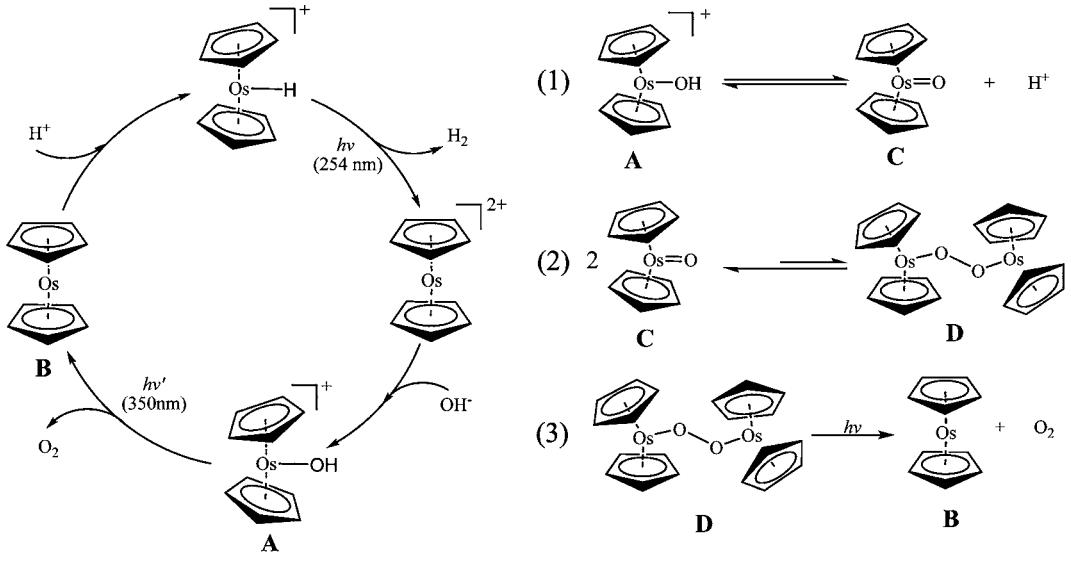

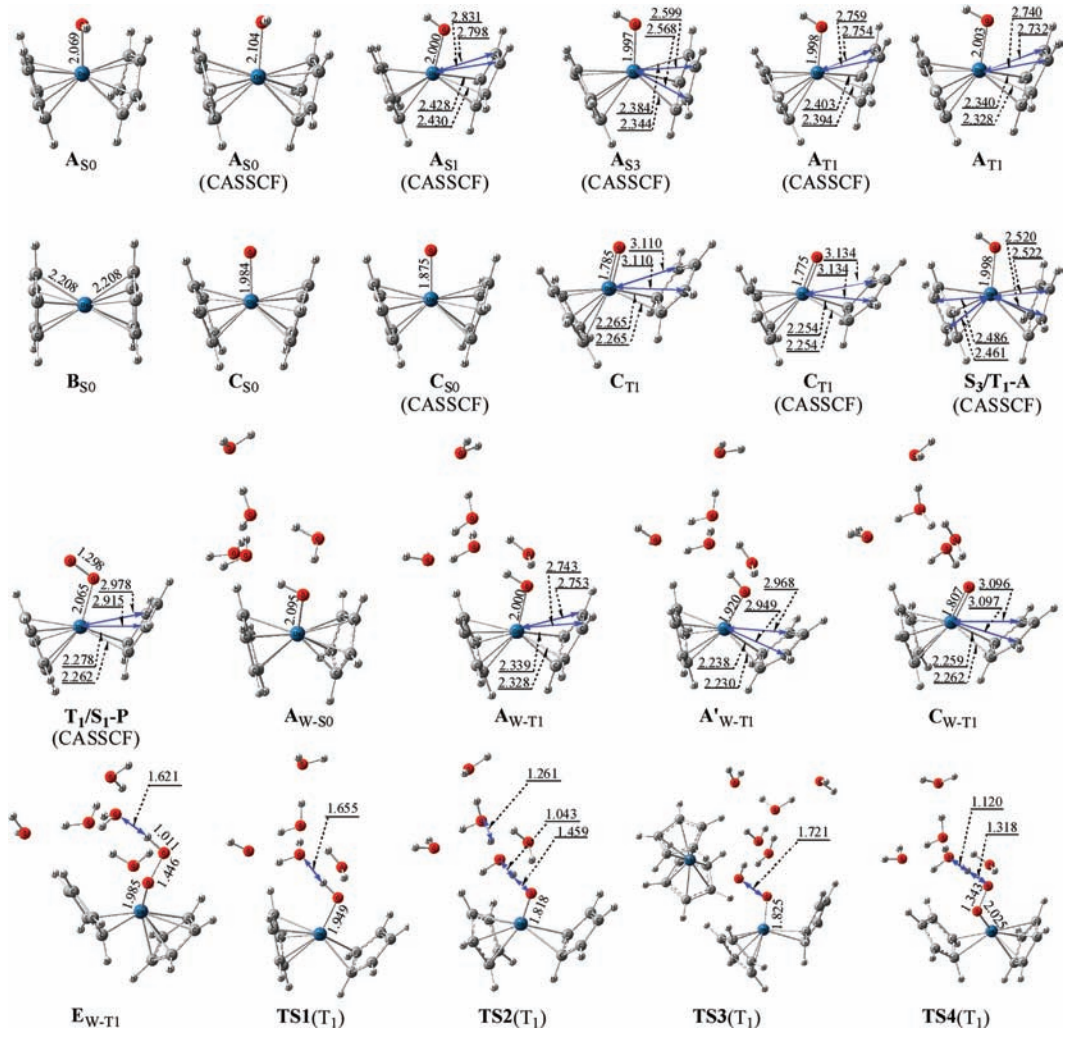

Figure 1. Stationary and intersection structures along with the selected bond distances (in Å). Structures optimized at the CASSCF level are labeled by (CASSCF), and the others are the result of CAM-B3LYP optimizations.

photochemical reactions are formally combined into an interesting cyclic process, as shown in Scheme 1,[36] which shows analogies to photosystem I and II of natural photosynthesis, where the reductive and oxidative parts also take place as

dx.doi.org/10.1021/ic202097c | Inorg. Chem. 2012, 51, 4938–4946

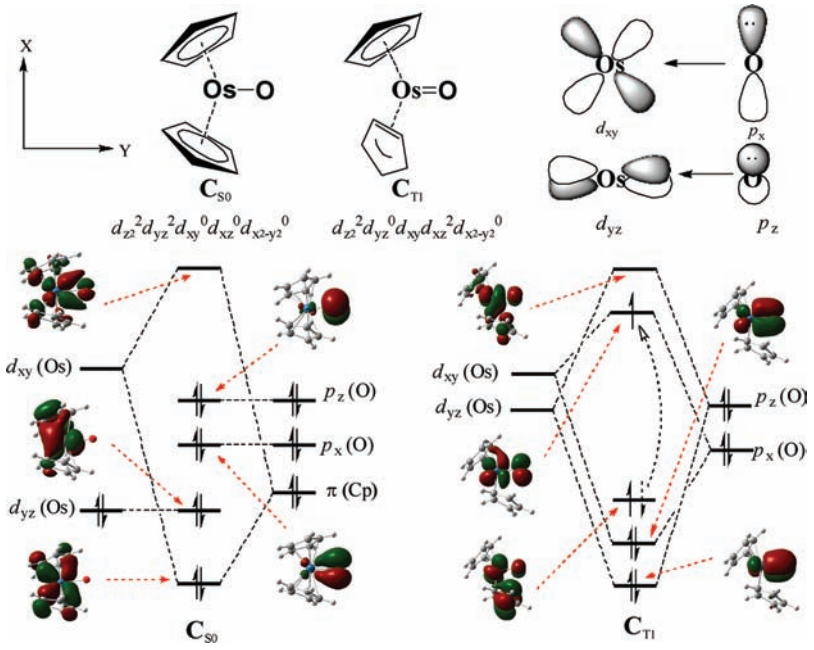

Figure 2. Molecular orbitals and electronic structures for the **C** complexes in the lowest singlet and triplet states.

separate processes. Deprotonation was suggested as the first step (step 1 in Scheme 1) for generating O_2 molecules from the $[Cp_2Os^{IV}OH]^+$ complex. However, it is unclear which state is involved in the deprotonation process, since the complex may be initially populated in an excited singlet state by photoexcitation. The second step proposed is the bimolecular reaction of two $[Cp_2Os^{IV}{=}O]$ complexes. However, the $[Cp_2Os^{IV}{=}O]$ complex is a transient intermediate produced by deprotonation of the $[Cp_2Os^{IV}OH]^+$ complex, and its concentration is probably very small. As a result, the bimolecular collision has little possibility of taking place. In addition, the singlet O_2 molecule was observed in the photolysis of the aqueous $[Cp_2Os^{IV}OH]^+$ complex. However, the precursor state for the $^1O_2$ formation was not explored in previous studies. These unsolved issues suggest that it is necessary to carry out a more detailed study on mechanism of O_2 generation with osmocene as photocatalyst.

There is a large body of studies related to photocatalytic water splitting into H_2 and O_2, but very few of them have been explored from a mechanistic perspective.[37] However, an understanding of the reaction mechanism is a fundamental piece of knowledge for the development of a practical technology to produce sunlight-derived hydrogen and oxygen. Therefore, there is an urgent need to characterize photocatalytic water-splitting pathways. It has been recognized that O_2 evolution is the major bottleneck,[7−20] hampering progress in the development of applicable devices for the conversion of sunlight into storable fuels. In the present work, we performed DFT (density functional theory), CASSCF (complete active space self-consistent field),[38,39] and CASPT2 (CASSCF second-order perturbation theory)[40,41] calculations to reveal the mechanism of photoinduced O_2 evolution promoted by osmocene complexes (**A** → **B** in Scheme 1). The stationary and intersection structures in the ground (S_0), the lowest triplet (T_1), and the excited singlet states (S_n, n = 1−3) were determined by DFT and CASSCF optimizations, and their relative energies were refined by CASPT2 calculations. Photoinduced O_2 evolution was predicted to involve nonadiabatic deprotonation, O−O bond formation, and subsequent nonadiabatic O_2 release. The present calculations provide new insights into the mechanism of water splitting by light with osmocene and related complexes as photocatalysts.

COMPUTATIONAL DETAILS

The geometric structures in the S_0 and T_1 states were optimized by using the long-range correction CAM-B3LYP functional[42] and were confirmed to be minima or first-order saddle points by the calculated vibrational frequencies. The stationary and intersection structures that involve the excited singlet state were determined by the CASSCF method. The active space for the CASSCF calculation is composed of 10 electrons in 8 orbitals, referred to as CAS(10,8) hereafter, which mainly originate from d orbitals of the Os atom and π orbitals of the Cp ligands. However, in a few cases, CAS(16,12) and CAS(12,9) calculations were performed, and the details for the active orbitals will be given in subsequent sections. On the basis of the CASSCF optimized structures, energies were corrected by single-point calculations at the CASPT2 level. The SDD basis set[43] was used for the Os atom and the cc-pVDZ basis set for all other atoms. This mixed basis set is used for all electronic structure calculations in the present study. The solvent effect was taken into account by a combination of the hydrogen-bonding interaction from explicit solvent molecules and effects from the bulk surrounding solvent molecules. The complex $[Cp_2Os^{IV}OH)]^+$ with five H_2O molecules is treated as the initial reactant for including the hydrogen-bonding interaction. To evaluate the importance of the bulk solvent effects added to the hydrogen-bonded complexes, we employed the self-consistent reaction field method to determine the structures and energies of the complexes. A dielectric constant of 78.4 is used for the water bulk using the polarizable continuum model (PCM), in which the cavity is created via a series of overlapping spheres. All DFT and CASSCF calculations were carried out using the Gaussian 09 program package[44] and the CASPT2 calculations using the Molcas 6.4 program package.[45]

RESULTS AND DISCUSSION

Deprotonation of the A Complex. The **A** complex in the ground state was optimized at the CAM-B3LYP level of theory, and the obtained structure, referred to as $\mathbf{A}_{S0}$, is shown in Figure 1 along with the key bond parameters. The two Cp rings are η^5 ligands in the $\mathbf{A}_{S0}$ structure and lie symmetrically below

dx.doi.org/10.1021/ic202097c | Inorg. Chem. 2012, 51, 4938−4946

and above the Os−O−H plane. The **A** complex in the S_0 state has C_s symmetry with an Os−O bond length of 2.069 Å at the CAM-B3LYP level. Deprotonation of the **A** complex in the S_0 state yields complex **C** (Scheme 1) in the closed-shell singlet state, and this process was characterized by the CAM-B3LYP calculations. The obtained structure is referred to as $\mathbf{C}_{S0}$ hereafter. The Os−O bond length is 1.984 Å in the $\mathbf{C}_{S0}$ structure, which is only slightly shorter than that in the $\mathbf{A}_{S0}$ structure. This gives us a hint that the Os−O bond in $\mathbf{C}_{S0}$ has single-bond character. The CAM-B3LYP calculated wave functions indicate that the Os atom in the $\mathbf{C}_{S0}$ complex has the electronic configuration $d_{z^2}^2 d_{yz}^2 d_{xy}^0 d_{xz}^0 d_{x^2-y^2}^0$, which is described in Figure 2. Since a strong interaction exists between the π orbitals of the Cp ligands and the d_{xy} orbital of the Os atom, there is little chance to form the $p_x^2-d_{xy}^0$ π bond between the O and Os atoms, which is the reason the Os−O bond has single-bond character in the $\mathbf{C}_{S0}$ complex. No transition state was found for the deprotonation process in the ground state, and the free energy is calculated to increase monotonously to 44.5 kcal/mol from $\mathbf{A}_{S0}$ to $\mathbf{C}_{S0}$ + $(H_2O)_4{\cdot}H_3O^+$ by using −11.803 eV as the free energy of the solvated proton.[25,28,46,47] This indicates that deprotonation from the **A** complex is rather difficult in the S_0 state.

The **A** and **C** complexes in the ground state were reoptimized at the CASSCF level, and the obtained structures are referred to as $\mathbf{A}_{S0}$(CASSCF) and $\mathbf{C}_{S0}$(CASSCF) in Figure 1, respectively. A comparison reveals that the CAM-B3LYP optimized bond parameters for the **A** complex in the S_0 state are very close to those from the CASSCF optimization. However, the CAM-B3LYP and CASSCF calculations give a noticeable difference in the Os−O bond length of the $\mathbf{C}_{S0}$ complex, which comes mainly from a different selection of the active space for the CASSCF optimization. Since the d_{z^2} orbital is always doubly occupied for the investigated complexes in the ground and excited states, the d_{z^2} orbital is not included in the active space for the present CASSCF calculation. For the **A** complex in the ground and excited states, the active space is composed of 10 electrons in 8 orbitals, which originates from four d orbitals (d_{yz}, d_{xy}, d_{xz}, and $d_{x^2-y^2}$) and four π orbitals (two π orbitals for each Cp group). The situation is slightly different for the **C** complex, and its lowest triplet state (T_1) exhibts a Os═O bond character, which will be discussed below. As a result, the p_x, p_y, and p_z orbitals of the O atom are added to the active space. As shown in Figure 1, the two Cp groups are not equivalent in the **C** complex in the T_1 state. One Cp π^* orbital has a slight interaction with the d_{xz} orbital, and this π^* is chosen as the acitve orbital. In total, 16 electrons in 12 orbitals are included in the active space for the CASSCF calculations of the **C** complex in the S_0 and T_1 states. Also, the CAS(12,9) optimizations were performed for the **C** complex with the one Cp π, p_y, and $d_{x^2-y^2}$ orbitals excluded from the CAS(16,12) active space. It was found that the CAS(12,9) optimized structures of the $\mathbf{C}_{S0}$ and $\mathbf{C}_{T1}$ complexes (see Figure 1) are similar to those from the CAS(16,12) optimizations in the Supporting Information. Therefore, the (12,9) active space is used for the subsequent CASSCF and CASPT2 calculations and nine active orbitals are depicted in Figure S1 of the Supporting Information. Generally speaking, the CAM-B3LYP optimized bond parameters for the ground and lowest triplet states are more reliable, while the CASSCF calculations can provide a balanced description of the ground- and excited-state structures.

In order to examine deprotonation of the **A** complex in an excited state, CAS(10,8) optimizations have been performed for several low-lying electronic states of the **A** complex. On the basis of the CASSCF optimized $\mathbf{A}_{S0}$ structure, the vertical excitation energies to the first three excited singlet states were calculated to be 2.32 eV (535 nm), 2.70 eV (459 nm), and 3.18 eV (389 nm) by using the CASPT2 method. The three excited states are all generated from the metal-centered (MC) d−d transitions ($d_{yz}-d_{x^2-y^2}$, $d_{yz}-d_{xy}$, $d_{yz}-d_{xz}$), and oscillator strengths are calculated to be 0.0030, 0.0021, and 0.0103, respectively. The $d_{yz}-d_{xz}$ transition is assigned to the absorption maximum at 405 nm (3.06 eV) measured for the **A** complex in aqueous solution.[36] Upon irradiation at 350 nm, the **A** complex is excited to the third excited singlet state (S_3) in the Franck−Condon (FC) region with some excess energy, which is followed by fast relaxation to its equilibrium structure. Structures of the **A** complex in the S_1, S_2, and S_3 states have been fully optimized at the CAS(10,8) level and their relative energies refined with the CASPT2 method. The CASSCF optimized S_3 structure is referred to as $\mathbf{A}_{S3}$(CASSCF) and is shown in Figure 1. The details for the optimized S_1, S_2, and S_3 structures can be found in the Supporting Information. Upon photoexcitation of the **A** complex from S_1 to S_3, one Cp ligand changes its binding fashion from η^5-Cp to η^3-Cp via ring slippage.[48−51] Two Os−C distances are increased by about 0.3 Å from $\mathbf{A}_{S0}$(CASSCF) to $\mathbf{A}_{S3}$(CASSCF). Such a ring slippage in the $\mathbf{A}_{S3}$(CASSCF) structure is attributed to a repulsive interaction between the unpaired d_{xz} electron and the Cp π electrons.

As discussed before, the deprotonation of the **A** complex is difficult in the ground state. The direct deprotonation for the **A** complex in the excited singlet states (S_1, S_2, and S_3) correlates adiabatically with the fragments in an excited singlet state and is of high endothermic character. Therefore, there is little possibility for the deprotonation to take place along the S_1, S_2, or S_3 pathway. However, the intersystem crossing (ISC) for the S_3 state to the T_1 state is expected to occur efficiently, due to a heavy atom effect in the **A** complex. The structure of the **A** complex in the T_1 state is obtained by the CASSCF optimization, labeled as $\mathbf{A}_{T1}$(CASSCF) hereafter. The CAS(10,8) calculated molecular orbitals and their electron populations indicate that the T_1 state originates from a metal-centered $d_{yz}-d_{xy}$ transition, which is different from the $d_{yz}-d_{xz}$ transition for the S_3 state. The $\mathbf{A}_{T1}$(CASSCF) structure has a η^3-Cp ligand with two Os−C distances elongated to 2.754 and 2.759 Å. The $S_3 \rightarrow T_1$ ISC process involves a transition from α spin to β spin and a change from the d_{xz} to the d_{xy} orbital. The ISC process can occur with high efficiency due to the conservation of the total (spin plus orbit) angular momentum.[52] The intersection structure between the S_3 and T_1 states has been determined by state-averaged CAS(10,8) optimizations and is referred to as $\mathbf{S_3/T_1}$-**A** in Figure 1, where the key bond parameters are given. Using a one-electron approximation for the spin−orbit coupling (SOC) operator with the effective nuclear charges, the SOC matrix elements between the S_3 and T_1 states were calculated to be 1885.3, 1250.8, and 819.8 cm^{-1} at the $\mathbf{A}_{S3}$(CASSCF), $\mathbf{S_3/T_1}$-**A**, and $\mathbf{A}_{T1}$(CASSCF) structures, respectively. The calculated results reveal that the spin−orbit interaction is very strong in the $\mathbf{A}_{S3}$(CASSCF) and $\mathbf{S_3/T_1}$-**A** structural regions. As shown in Figure 3, the energy difference between $\mathbf{A}_{S3}$(CASSCF) and $\mathbf{S_3/T_1}$-**A** is very small (2.8 kcal/mol). In addition, the $\mathbf{A}_{S3}$(CASSCF) structure is similar to that for the $\mathbf{S_3/T_1}$-**A** intersection. All these results give strong

dx.doi.org/10.1021/ic202097c | Inorg. Chem. 2012, 51, 4938−4946

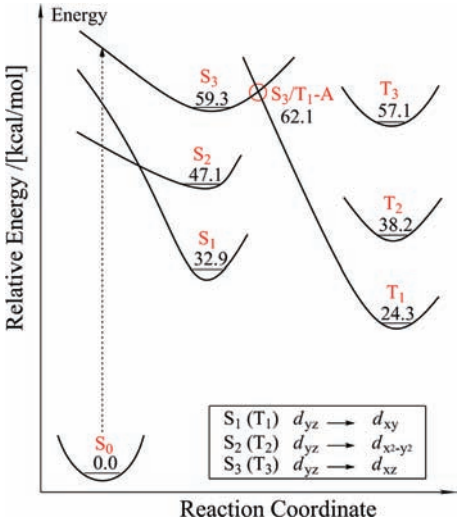

Figure 3. Relative energies of the minimum-energy and intersection structures for the **A** complex in the excited singlet and triplet states, calculated at the CASPT2//CASSCF level.

evidence that the $S_3 \rightarrow T_1$ ISC process occurs with high efficiency.

It should be pointed out that the **A** complex in the S_3 state can decay to the T_1 state through the $S_3 \rightarrow S_1$ internal conversion and the subsequent $S_1 \rightarrow T_1$ ISC process. As discussed before, both the S_1 and T_1 states come from the same MC $d_{yz} \rightarrow d_{xy}$ transition, and they have the same electronic configuration of $(...d_{yz}^1 d_{xy}^1)$. The $S_1 \rightarrow T_1$ ISC process only involves the spin flip of one d electron, and there is no change in the orbital angular momentum in this process. The $S_1 \rightarrow T_1$ ISC process for the **A** complex occurs with little possibility because the total angular momentum is not conserved for the $S_1 \rightarrow T_1$ transition. Upon photoexcitation at 350 nm, the most possible photophysical processes and the related electronic states are summarized in Figure 3, where the relative energies are given for the stationary and intersection structures.

Deprotonation of the **A** complex along the T_1 pathway was characterized by CAM-B3LYP and CASSCF calculations. The CAM-B3LYP optimized structures for **A** and **C** in the T_1 state are respectively referred to as $\mathbf{A}_{T1}$ and $\mathbf{C}_{T1}$ in Figure 1 along with the selected bond parameters. The Os−O bond length in $\mathbf{A}_{T1}$ is 2.003 Å at the CAM-B3LYP level, which is very close to that of 1.998 Å obtained by the CAS(10,8) calculations. As discussed above, the T_1 state comes from the MC d_{yz}−d_{xy} transition for the **A** complex. This MC transition has little influence on the Os−O bond nature. Thus, the Os−O single-bond character is not changed from S_0 to T_1 for the **A** complex. However, the Os−O bond has double-bond character in the $\mathbf{C}_{T1}$ structure with Os−O distances of 1.785 and 1.775 Å at the CAM-B3LYP and CAS(12,9) levels of theory. The CAS(12,9) and CAM-B3LYP calculated wave functions indicate that the Os atom in the $\mathbf{C}_{T1}$ structure has the electronic configuration $d_{z^2}^2 d_{xz}^2 d_{yz}^0 d_{xy}^0 d_{x^2-y^2}^0$ with unoccupied d_{yz} and d_{xy} orbitals, as shown in Figure 2. There exists a noticeable d−p interaction between the Os and O atoms. In addition, the $\mathbf{C}_{T1}$ electronic structure exhibits a partial charge-transfer character from the π orbital of the Cp ring to the d_{xy}−p_x π^* orbital. As a result, there is one η^2-Cp ligand in the $\mathbf{C}_{T1}$ complex, in addition to the Os═O double-bond nature. With respect to the S_0 minimum, the $\mathbf{A}_{T1}$ complex has relative energies of 25.9 and 24.3 kcal/mol at the CAM-B3LYP and CASPT2/CASSCF levels of theory, respectively.

For a better description of the deprotonation process in aqueous solution, five water molecules were put into the reaction system and the **A** complex with explicit waters is denoted as $\mathbf{A}_W$. The CAM-B3LYP optimized structures for the $\mathbf{A}_W$ complexes in the S_0 and T_1 states are referred to as $\mathbf{A}_{W\text{-}S0}$ and $\mathbf{A}_{W\text{-}T1}$ respectively. As can be seen from Figure 4, the

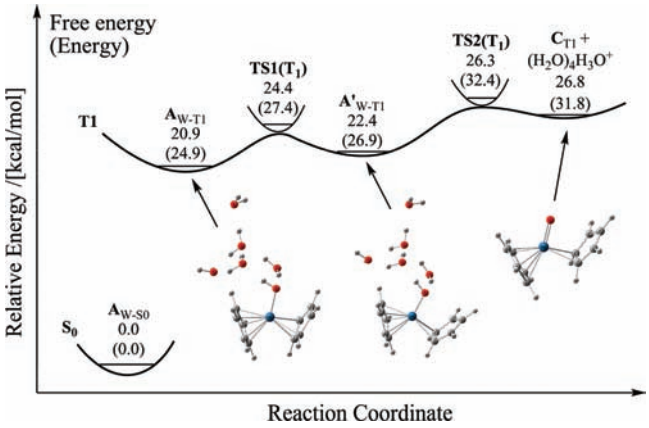

Figure 4. Free energy profile for deprotonation of the **A** complex on the T_1 pathway along with the CAM-B3LYP calculated energies (in parentheses) and free energies relative to the **A** complex in the ground state.

relative free energy of $\mathbf{A}_{W\text{-}T1}$ is 20.9 kcal/mol, which is about 4.0 kcal/mol lower than its relative energy. The CAM-B3LYP calculations reveal that the T_1 deprotonation involves an intermediate of $\mathbf{A'}_{W\text{-}T1}$ and the process can be represented as $\mathbf{A}_{W\text{-}T1} \rightarrow \mathbf{TS1}(T_1) \rightarrow \mathbf{A'}_{W\text{-}T1} \rightarrow \mathbf{TS2}(T_1) \rightarrow \mathbf{C}_{T1} + (H_2O)_4{\cdot}H_3O^+$. The optimized structures for the intermediate and transition states are shown in Figure 1, and the calculated relative energies and free energies are given in Figure 4. The first step is the isomerization from $\mathbf{A}_{W\text{-}T1}$ to $\mathbf{A'}_{W\text{-}T1}$ and has an activation free energy of 3.5 kcal/mol, which is close to that of 3.9 kcal/mol for the second step of the deprotonation. The calculated results clearly show that deprotonation of the **A** complex proceeds very easily along the T_1 pathway.

O−O Bond Formation. O−O bond formation has been suggested through direct oxo−oxo coupling, as described in step 2 of Scheme 1. The direct coupling of two **C** complexes in the lowest singlet and triplet states might yield the **D** complexes in the quintet, triplet, and open- and closed-shell singlet states. All attempts to optimize the minimum-energy structure for the **D** complex in the closed-shell singlet state lead to formation of the $\mathbf{B}_{S0}$ and $\mathbf{F}_{S0}$ complexes. As shown in Figure 5, the transition state of $\mathbf{TSD}_{S0}$ is found on the pathway from $2\mathbf{C}_{S0}$ to $\mathbf{B}_{S0} + \mathbf{F}_{S0}$ by the CAM-B3LYP optimizations and $\mathbf{TSD}_{S0}$ has a relative free energy of 128.4 kcal/mol. The symmetry-breaking technique was used to optimize the minimum-energy structure of the **D** complex, which shows that the **D** complex in the ground state has open-shell singlet character, referred to as $\mathbf{D}_{SU}$ hereafter. A transition state, $\mathbf{TSD}_{SU}$, was determined on the pathway from $2\mathbf{C}_{T1}$ to $\mathbf{D}_{SU}$, and the active free energy was predicted to be 107.1 kcal/mol. Instead of formation of the **D** complex in the triplet state, $2\mathbf{B}_{S0} + {}^3O_2$ were determined as the products on the triplet-state pathway with an activation free energy of 119.1 kcal/mol. The **D** complexes in the quintet state, referred to as $\mathbf{D}_Q$ in Figure 5, can be formed from the

dx.doi.org/10.1021/ic202097c | Inorg. Chem. 2012, 51, 4938−4946

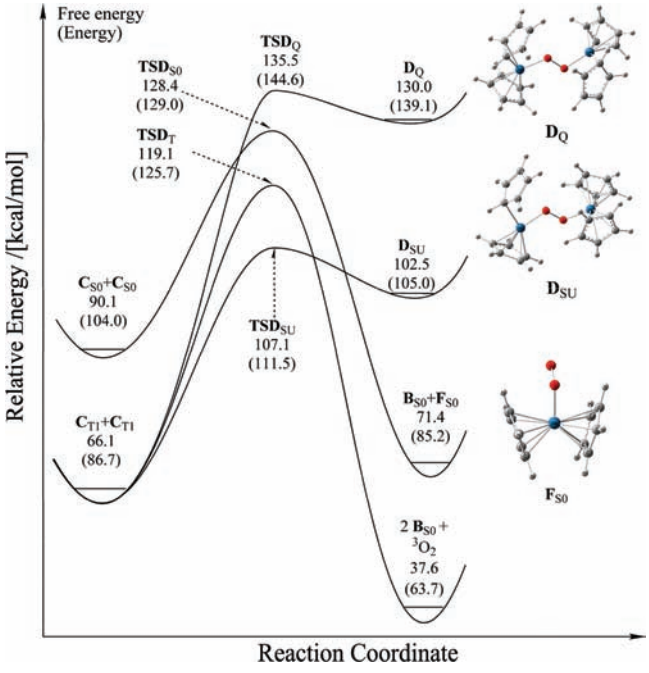

Figure 5. Free energy profiles for the bimolecular **C** + **C** reactions in different states along with the CAM-B3LYP calculated energies (in parentheses) and free energies relative to the **A** complex in the ground state.

bimolecular $\mathbf{C}_{T1}$ + $\mathbf{C}_{T1}$ reaction, which is endothermic by 139.1 kcal/mol with an activation free energy of 135.5 kcal/mol. With respect to the **A** complex in the S_0 state, the activation free energies were calculated to be in the range 107.1−135.5 kcal/mol for the bimolecular **C** + **C** reactions in the lowest singlet and triplet states. Actually, these processes are inaccessible in energy upon photoexcitation at 350 nm. The present calculation reveals that the O−O bond has little possibility of forming by the direct coupling of two **C** complexes.

In addition, the **C** complex is the intermediate produced by deprotonation of the aqueous **A** complexes and the probability of two **C** complexes colliding with each other is very small. If the **D** complex was formed as the stable intermediate from the bimolecular **C** + **C** reaction, the **D** complex should be detected experimentally. As an example, photolysis of the (Pcts)-$Fe^{III}(O_2^{2-})Fe^{III}$(Pcts) complex ($PctsH_2$ = phthalocyaninetetrasulfonate) leads to O_2 release and this complex was observed by the spectral changes to persist for some 1.0 h.[53] However, there is no direct experimental evidence for formation of the **D** complex for the present osmium complex in aqueous solution.[36]

A new pathway is proposed for formation of the O−O bond here, in which the **C** complex in the T_1 state reacts initially with the $\mathbf{A}_W$ complex in the S_0 state. This process is generally classified as the acid−base mechanism in previous studies.[26,28,37] A complex of $Cp_2OsOOH^+\cdot(H_2O)_5$ in the triplet state, referred to as $\mathbf{E}_{W\text{-}T1}$ hereafter, is produced through the transition state $\mathbf{TS3}(T_1)$. This process can be represented as $\mathbf{A}_{W-S0}$ + $\mathbf{C}_{T1}$ → $\mathbf{TS3}(T_1)$ → $\mathbf{B}_{S0}$ + $\mathbf{E}_{W\text{-}T1}$. From the optimized structure of $\mathbf{E}_{W\text{-}T1}$ in Figure 1, it can be seen that the O−O single bond is formed in the $\mathbf{E}_{W\text{-}T1}$ complex with an O−O distance of 1.426 Å at the CAM-B3LYP level. In addition, the Os−O bond exhibits a single-bond character with an Os−O distance of 1.985 Å in the $\mathbf{E}_{W\text{-}T1}$ complex, which gives us a hint that the Os−O bond is broken easily, and this will be discussed below. As shown in Figure 6, the relative free energy of $\mathbf{TS3}(T_1)$ is predicted to be 90.4 kcal/mol for formation of the

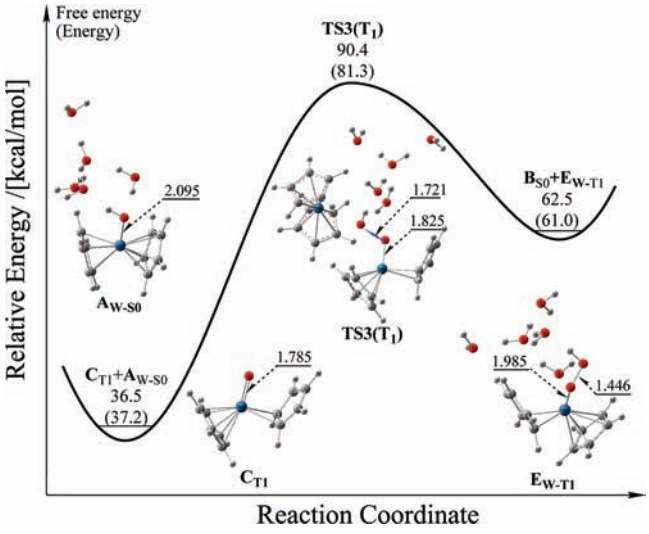

Figure 6. Free energy profiles for O−O bond formation in the $\mathbf{E}_{W\text{-}T1}$ complex along with the key stationary structures and the CAM-B3LYP calculated energies (in parentheses) and free energies relative to the **A** complex in the ground state.

O−O bond in the $\mathbf{E}_{W\text{-}T1}$ complex, which is much lower than those (107−135 kcal/mol) on the bimolecular **C** + **C** pathways discussed before.

The water nucleophilic attack at the **C** complex is a possible channel for forming the O−O bond,[21,28,37] which has been explored by the CAM-B3LYP calculations. The calculated results are summarized in Figure 7, where the related stationary

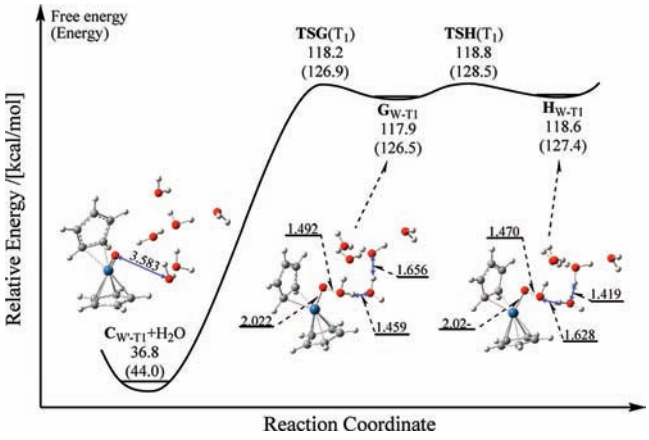

Figure 7. Free energy profiles for the O−O bond formation via the water nucleophilic attack mechanism along with the key stationary structures and the CAM-B3LYP calculated energies (in parentheses) and free energies relative to the **A** complex in the ground state.

structures and their relative free energies are given. First, the H_2O nucleophilic attack at the $\mathbf{C}_{W'\text{-}T1}$ complex leads to formation of an intermediate ($\mathbf{G}_{W\text{-}T1}$) through the transition state $\mathbf{TSG}(T_1)$. Subsequently, the water oxidation is completed by proton and electron transfers. With respect to the $\mathbf{A}_{S0}$ minimum, the activated free energy was predicted to be 118.2 kcal/mol by CAM-B3LYP calculations for the first step from $\mathbf{C}_{W'\text{-}T1}$ + H_2O to $\mathbf{G}_{W\text{-}T1}$, which is much higher than the

dx.doi.org/10.1021/ic202097c | Inorg. Chem. 2012, 51, 4938−4946

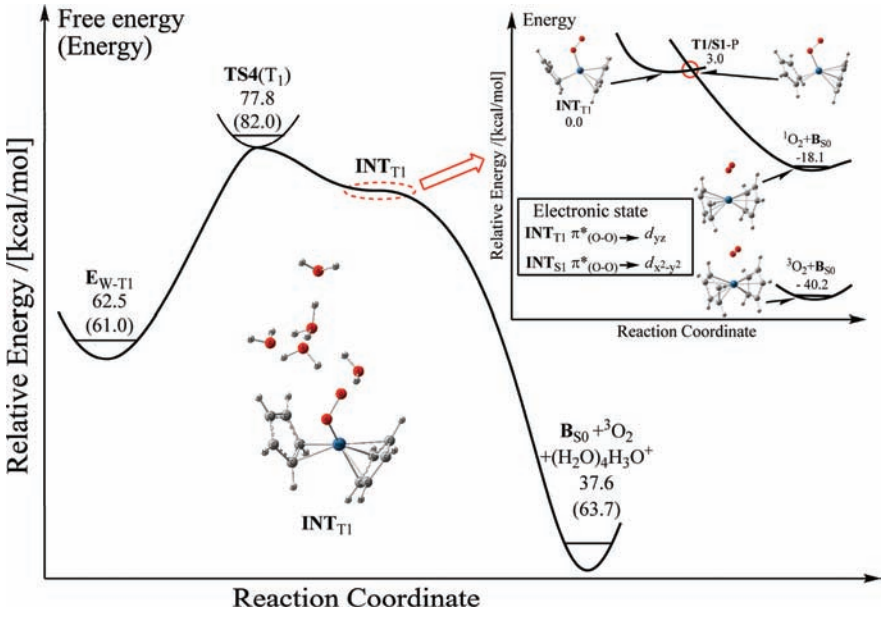

Figure 8. Free energy profiles for $^1O_2$ and $^3O_2$ release from the $\mathbf{E}_{W\text{-}T1}$ complex along with the CAM-B3LYP calculated energies (in parentheses) and free energies relative to the **A** complex in the ground state. Information related to the triplet−singlet intersection is given in the inset, where the relative energies were calculated at the CASPT2//CASSCF level.

activation free energy of 90.4 kcal/mol on the acid−base pathway from $\mathbf{A}_{W\text{-}S0}$ + $\mathbf{C}_{T1}$ to $\mathbf{B}_{S0}$ + $\mathbf{E}_{W\text{-}T1}$. It is evident that O−O bond formation via water nucleophilic attack is not in competition with that through the acid−base mechanism.

O_2 Release from the $E_{W\text{-}T1}$ Complex. O_2 release from the $\mathbf{E}_{W\text{-}T1}$ complex was investigated by combined CAM-B3LYP and CASSCF calculations. The transition state **TS4**(T_1) was found on the T_1 pathway for the O_2 release, and the activation free energy is 15.3 kcal/mol at the CAM-B3LYP level for this process. The **TS4**(T_1) transition state has a free energy of 77.8 kcal/mol with respect to the $\mathbf{A}_W$ complex in the ground state. The O−H bond is nearly broken in the **TS4**(T_1) structure, while the Os−O distance is increased by 0.04 Å from $\mathbf{E}_{W\text{-}T1}$ to **TS4**(T_1). The Os−O and O−H cleavages can be considered as an asynchronous concerted process. As a result, the free energy surface is very flat in the Os−O range of 2.04−2.14 Å. More importantly, the triplet−singlet intersection ($\mathbf{T_1/S_1}$**-P**) was found in this flat region by state-averaged CAS(12,9) calculations (see the inset of Figure 8). In the CAS(12,9) optimization of the $\mathbf{T_1/S_1}$**-P** structure, the Os−O σ and σ^* orbitals, two p orbitals of the O atom, two π orbitals (one for each Cp group), and three d orbitals (d_{yz}, d_{xy}, and d_{xz}) were included in the active space. The CAS(12,9) calculated wave function and the SOC matrix elements show that triplet → singlet intersystem crossing takes place with high efficiency in the vicinity of the $\mathbf{T_1/S_1}$**-P** intersection. As shown in the inset of Figure 8, the lowest singlet state is repulsive with the Os−O distance. Once the system relaxes to this state, the singlet O_2 molecule is released immediately. The combined CAM-B3LYP and CASSCF calculations reveal that the molecular oxygen is released easily from the $\mathbf{E}_{W\text{-}T1}$ complex and the formed O_2 molecule is either in the singlet state or in the triplet state. It should be pointed out that the formed $^3O_2$ molecule can be converted into the $^1O_2$ molecule by the heavy-atom effect from the Os complexes. In the photolysis of the **A** complex in aqueous solution, molecular oxygen was observed in the singlet state.[36] As discussed before, deprotonation of the $\mathbf{A}_{W\text{-}T1}$ complex takes place very easily. Thus, formation of the O−O bond is the rate-determining step for the generation of molecular oxygen. With respect to the $\mathbf{A}_{W\text{-}S0}$ complex, O−O bond formation has an energy barrier of 81.3 kcal/mol, which is accessible in energy upon photoexcitation of the aqueous **A** complex at 350 nm (~82 kcal/mol). Since O_2 release is a nonadiabatic process and involves several sequential steps, the O_2 molecule is generated with low efficiency, which is consistent with the quantum yield of 2×10^{-3} observed for the disappearance of aqueous **A** complexes.

SUMMARY

Photoinduced O_2 evolution from the $[Cp_2Os{-}OH]^+$ complex in aqueous solution has been studied by DFT, CASSCF, and CASPT2 methods. O_2 formation was predicted to be composed of three consecutive steps: deprotonation, formation of the O−O bond, and O_2 release, which are consistent with those suggested in the experimental study. The S_3 state is initially populated upon photolysis of the aqueous $[Cp_2Os{-}OH]^+$ complex, and this assignment is based on a comparison of the CASPT2//CASSCF calculated excitation energies and oscillator strengths with the first absorption maximum at 405 nm observed experimentally. Direct deprotonation from the S_3 state of the $\mathbf{A}_W$ complex has little possibility of occurring, due to its endothermic character, which is not in competition with internal conversion to the S_0 state or intersystem crossing to the T_1 state. The optimized $\mathbf{S_3/T_1}$**-A** intersection structure, the calculated SOC matrix elements, and the energy difference between the S_3 and T_1 states provide strong evidence that the $S_3 \rightarrow T_1$ intersystem crossing occurs with high efficiency. The deprotonation free energy of the $\mathbf{A}_W$ complex in the S_0 state is 44.5 kcal/mol at the CAM-B3LYP level, while the deprotonation from the T_1 state of the $\mathbf{A}_W$ complex has an activation free energy of less than 4.0 kcal/mol and proceeds very easily. In addition, the $\mathbf{C}_W$ complex in the T_1 state produced by deprotonation of the $\mathbf{A}_{W\text{-}T1}$ complex is about 20.0 kcal/mol lower than the $\mathbf{C}_{W\text{-}S0}$ complex in energy. The present calculation indicates that the first step of deprotonation should

dx.doi.org/10.1021/ic202097c | Inorg. Chem. 2012, 51, 4938−4946

occur along the T_1 pathway as a result of efficient $S_3 \rightarrow T_1$ intersystem crossing.

O−O bond formation has been suggested to occur through direct oxo−oxo coupling, but no experimental evidence was given in the previous study. The bimolecular **C** + **C** reactions in the lowest singlet and triplet states can give birth to the **D** complexes in different electronic states. However, these reactions have their activation free energies in the range of 107.0−135.5 kcal/mol with respect to the **A** complex in the ground state, which are inaccessible in energy upon photoexcitation of the **A** complex at 350 nm. In addition, the **C** complex is the intermediate produced by deprotonation, and there is little possibility of two **C** complexes colliding with each other. If the **D** complex is formed as the stable intermediate from the bimolecular **C** + **C** reaction, the **D** complex should be detected experimentally. The present calculation reveals that the O−O bond has little possibility of forming from the direct coupling of two **C** complexes and does not support the mechanism suggested in the previous study. O−O bond formation via water nucleophilic attack at the **C** complex was also explored by the CAM-B3LYP calcualtions. The activation free energy was predicted to be 118.2 kcal/mol at the first step of the water nucleophilic attack reaction, which indicates that the reaction has little possibility of proceeding upon irradiation at 350 nm.

We examined the acid−base mechanism where the hydroxyl oxygen of $\mathbf{A}_{W\text{-}S0}$ attacks the $\mathbf{C}_{T1}$ oxygen, forming a triplet complex of $\mathbf{E}_{W\text{-}T1}$ with the −OOH group. In addition to formation of the O−O single bond, the Os−O bond exhibits a single-bond character in the $\mathbf{E}_{W\text{-}T1}$ complex, which favors of the subsequent cleavage of the Os−O bond. O_2 release from the $\mathbf{E}_{W\text{-}T1}$ complex was predicted to be an asynchronous concerted cleavage of the Os−O and O−H bonds and has to overcome a free energy barrier of 15.3 kcal/mol first. Then the $\mathbf{T_1/S_1}$**-P** intersection was found on the pathway to the O_2 molecule. The formed O_2 molecule is either in the lowest singlet state or in the lowest triplet state. In the photolysis of the **A** complex in aqueous solution, molecular oxygen was observed in the singlet state. The formed $^3O_2$ molecule can be converted into the $^1O_2$ molecule by the heavy atom effect from the Os complexes, which is probably the reason the $^3O_2$ molecule was not detected experimentally. The combined CAM-B3LYP and CASSCF calculations reveal that deprotonation of the $\mathbf{A}_{W\text{-}T1}$ complex and O_2 release from the $\mathbf{E}_{W\text{-}T1}$ complex take place very easily. Formation of the O−O bond is the rate-determining step for the photolysis of the **A** complex in aqueous solution to generate molecular oxygen. With respect to the $\mathbf{A}_{W\text{-}S0}$ complex, O−O bond formation has an activation energy of 81.3 kcal/mol, which is accessible in energy upon photoexcitation of the aqueous **A** complex at 350 nm (~82 kcal/mol). Since O_2 release is a nonadiabatic process and involves several sequential steps, the O_2 molecule is generated with low quantum field.

■ ASSOCIATED CONTENT

Ⓢ Supporting Information

Tables and figures giving Cartesian coordinates and energies of the stationary structures. This material is available free of charge via the Internet at http://pubs.acs.org.

■ AUTHOR INFORMATION

Corresponding Author

*E-mail: Fangwh@bnu.edu.cn.

Notes

The authors declare no competing financial interest.

■ ACKNOWLEDGMENTS

This work was supported by grants from the NSFC (Grant Nos. 20720102038 and 21033002) and from the Major State Basic Research Development Programs (Grant No. 2011CB808503).

■ REFERENCES

(1) Messinger, J. *ChemSusChem* **2009**, *2*, 47−48.
(2) Concepcion, J. J.; Jurss, J. W.; Templeton, J. L.; Meyer, T. J. *Proc. Natl. Acad. Sci. U.S.A.* **2008**, *105*, 17632−17635.
(3) Yagi, M.; Syouji, A.; Yamada, S.; Komi, M.; Yamazaki, H.; Tajima, S. *Photochem. Photobiol. Sci.* **2009**, *8*, 139−147.
(4) Eisenberg, R.; Gray, H. B. *Inorg. Chem.* **2008**, *47*, 1697−1699.
(5) Tinker, L. L.; McDaniel, N. D.; Bernhard, S. *J. Mater. Chem.* **2009**, *19*, 3328−3337.
(6) Crittenden, J. C.; White, H. S. *J. Am. Chem. Soc.* **2010**, *132*, 4503−4505.
(7) Tagore, R.; Crabtree, R. H.; Brudvig, G. W. *Inorg. Chem.* **2008**, *47*, 1815−1823.
(8) Liu, F.; Concepcion, J. J.; Jurss, J. W.; Cardolaccia, T.; Templeton, J. L.; Meyer, T. J. *Inorg. Chem.* **2008**, *47*, 1727−1752.
(9) Concepcion, J. J.; Jurss, J. W.; Templeton, J. L.; Meyer, T. J. *J. Am. Chem. Soc.* **2008**, *130*, 16462−16463.
(10) Geletii, Y. V.; Botar, B.; Kögerler, P.; Hillesheim, D. A.; Musaev, D. G.; Hill, C. L. *Angew. Chem., Int. Ed.* **2008**, *47*, 3896−3899.
(11) McDaniel, N. D.; Coughlin, F. J.; Tinker, L. L.; Bernhard, S. *J. Am. Chem. Soc.* **2007**, *130*, 210−217.
(12) Limburg, J.; Vrettos, J. S.; Liable-Sands, L. M.; Rheingold, A. L.; Crabtree, R. H.; Brudvig, G. W. *Science* **1999**, *283*, 1524−1527.
(13) Tseng, H.-W.; Zong, R.; Muckerman, J. T.; Thummel, R. *Inorg. Chem.* **2008**, *47*, 11763−11773.
(14) Yagi, M.; Kaneko, M. *Chem. Rev.* **2000**, *101*, 21−36.
(15) Cady, C. W.; Crabtree, R. H.; Brudvig, G. W. *Coord. Chem. Rev.* **2008**, *252*, 444−455.
(16) Yamazaki, H.; Shouji, A.; Kajita, M.; Yagi, M. *Coord. Chem. Rev.* **2010**, *254*, 2483−2491.
(17) Sala, X.; Romero, I.; Rodríguez, M.; Escriche, L.; Llobet, A. *Angew. Chem., Int. Ed.* **2009**, *48*, 2842−2852.
(18) Brimblecombe, R.; Dismukes, G. C.; Swiegers, G. F.; Spiccia, L. *Dalton Trans.* **2009**, 9374−9384.
(19) Dau, H.; Limberg, C.; Reier, T.; Risch, M.; Roggan, S.; Strasser, P. *ChemCatChem* **2010**, *2*, 724−761.
(20) Gersten, S. W.; Samuels, G. J.; Meyer, T. J. *J. Am. Chem. Soc.* **1982**, *104*, 4029−4030.
(21) Concepcion, J. J.; Tsai, M.-K.; Muckerman, J. T.; Meyer, T. J. *J. Am. Chem. Soc.* **2010**, *132*, 1545−1557. Polyansky, D. E.; Muckerman, J. T.; Rochford, J.; Zong, R.; Thummel, R. P.; Fujita, E. *J. Am. Chem. Soc.* **2011**, *133*, 14649−14665.
(22) Hurst, J. K.; Cape, J. L.; Clark, A. E.; Das, S.; Qin, C. *Inorg. Chem.* **2008**, *47*, 1753−1764.
(23) Yamada, H.; Siems, W. F.; Koike, T.; Hurst, J. K. *J. Am. Chem. Soc.* **2004**, *126*, 9786−9795.
(24) Cape, J. L.; Siems, W. F.; Hurst, J. K. *Inorg. Chem.* **2009**, *48*, 8729−8735.
(25) Yang, X.; Baik, M.-H. *J. Am. Chem. Soc.* **2008**, *130*, 16231−16240.
(26) Nyhlén, J.; Duan, L.; Åkermark, B.; Sun, L.; Privalov, T. *Angew. Chem., Int. Ed.* **2010**, *49*, 1773−1777.
(27) Kuznetsov, A. E.; Geletii, Y. V.; Hill, C. L.; Morokuma, K.; Musaev, D. G. *J. Am. Chem. Soc.* **2009**, *131*, 6844−6854.
(28) Wang, L.-P.; Wu, Q.; Van Voorhis, T. *Inorg. Chem.* **2010**, *49*, 4543−4553.
(29) Yang, X.; Baik, M.-H. *J. Am. Chem. Soc.* **2006**, *128*, 7476−7485.

(30) Kohl, S. W.; Weiner, L.; Schwartsburd, L.; Konstantinovski, L.; Shimon, L. J. W.; Ben-David, Y.; Iron, M. A.; Milstein, D. *Science* **2009**, *324*, 74−77.
(31) Yang, X.; Hall, M. B. *J. Am. Chem. Soc.* **2009**, *132*, 120−130.
(32) Li, J.; Shiota, Y.; Yoshizawa, K. *J. Am. Chem. Soc.* **2009**, *131*, 13584−13585.
(33) Chen, Y.; Fang, W.-H. *J. Phys. Chem. A* **2010**, *114*, 10334−10338.
(34) Hetterscheid, D. G. H.; van der Vlugt, J. I.; de Bruin, B.; Reek, J. N. H. *Angew. Chem., Int. Ed.* **2009**, *48*, 8178−8181.
(35) Eisenberg, R. *Science* **2009**, *324*, 44−45.
(36) Kunkely, H.; Vogler, A. *Angew. Chem., Int. Ed.* **2009**, *48*, 1685−1687.
(37) Romain, S.; Vigara, L.; Llobet, A. *Acc. Chem. Res.* **2009**, *42*, 1944−1953.
(38) Roos, B. O.; Taylor, P. R.; Siegbahn, P. E. M. *Chem. Phys.* **1980**, *48*, 157−173.
(39) Frisch, M.; Ragazos, I. N.; Robb, M. A.; Bernhard Schlegel, H. *Chem. Phys. Lett.* **1992**, *189*, 524−528. Yamamoto, N.; Vreven, T.; Robb, M. A.; Frisch, M. J.; Schlegel, H. B. *Chem. Phys. Lett.* **1996**, *250*, 373−378.
(40) Andersson, K.; Malmqvist, P.-Å.; Roos, B. O. *J. Chem. Phys.* **1992**, *96*, 1218−1226.
(41) Andersson, K.; Malmqvist, P. A.; Roos, B. O.; Sadlej, A. J.; Wolinski, K. *J. Phys. Chem.* **1990**, *94*, 5483−5488.
(42) Yanai, T.; Tew, D. P.; Handy, N. C. *Chem. Phys. Lett.* **2004**, *393*, 51−57.
(43) Dolg, M.; Wedig, U.; Stoll, H.; Preuss, H. *J. Chem. Phys.* **1987**, *86*, 866−872. Kendall, R. A.; T. H. Dunning, J.; Harrison, R. J. *J. Chem. Phys.* **1992**, *96*, 6796−6806.
(44) Frisch, M. J.; Trucks, G. W.; Schlegel, H. B.; Scuseria, G. E.; Robb, M. A.; Cheeseman, J. R.; Scalmani, G.; Barone, V.; Mennucci, B.; Petersson, G. A.; Nakatsuji, H.; Caricato, M.; Li, X.; Hratchian, H. P.; Izmaylov, A. F.; Bloino, J.; Zheng, G.; Sonnenberg, J. L.; Hada, M.; Ehara, M.; Toyota, K.; Fukuda, R.; Hasegawa, J.; Ishida, M.; Nakajima, T.; Honda, Y.; Kitao, O.; Nakai, H.; Vreven, T.; Montgomery, J. A., Jr.; Peralta, J. E.; Ogliaro, F.; Bearpark, M.; Heyd, J. J.; Brothers, E.; Kudin, K. N.; Staroverov, V. N.; Kobayashi, R.; Normand, J.; Raghavachari, K.; Rendell, A.; Burant, J. C.; Iyengar, S. S.; Tomasi, J.; Cossi, M.; Rega, N.; Millam, J. M.; Klene, M.; Knox, J. E.; Cross, J. B.; Bakken, V.; Adamo, C.; Jaramillo, J.; Gomperts, R.; Stratmann, R. E.; Yazyev, O.; Austin, A. J.; Cammi, R.; Pomelli, C.; Ochterski, J. W.; Martin, R. L.; Morokuma, K.; Zakrzewski, V. G.; Voth, G. A.; Salvador, P.; Dannenberg, J. J.; Dapprich, S.; Daniels, A. D.; Farkas, O.; Foresman, J. B.; Ortiz, J. V.; Cioslowski, J.; Fox, D. J. *Gaussian 09*; Gaussian, Inc., Wallingford, CT, 2009.
(45) Karlström, G.; Lindh, R.; Malmqvist, P. Å.; Roos, B. O.; Ryde, U.; Veryazov, V.; Widmark, P.-O.; Cossi, M.; Schimmelpfennig, B.; Neograd y, P.; Seijo, L. *Comput. Mater. Sci.* **2003**, 28.
(46) Tissandier, M. D.; Cowen, K. A.; Feng, W. Y.; Gundlach, E.; Cohen, M. H.; Earhart, A. D.; Coe, J. V.; Tuttle, T. R. *J. Phys. Chem. A* **1998**, *102*, 7787−7794.
(47) Tawa, G. J.; Topol, I. A.; Burt, S. K.; Caldwell, R. A.; Rashin, A. A. *J. Chem. Phys.* **1998**, *109*, 4852−4863.
(48) Calhorda, M. J.; Veiros, L. F. *Coord. Chem. Rev.* **1999**, *185*−*186*, 37−51.
(49) O'Connor, J. M.; Casey, C. P. *Chem. Rev.* **1987**, *87*, 307−318.
(50) Ariafard, A.; Tabatabaie, E. S.; Yates, B. F. *J. Phys. Chem. A* **2009**, *113*, 2982−2989.
(51) Veiros, L. F. *Organometallics* **2000**, *19*, 5549−5558.
(52) Turro, N. J.; Ramamurthy, V.; Scaiano, J. C. *Modern Molecular Photochemistry of Organic Molecules*; University Science Books; Mill Valley, CA, 2010.
(53) Vogler, A.; Kunkely, H. *Coord. Chem. Rev.* **2006**, *250*, 1622−1626.